4.1.2.4 Faculae and plage

Sami Solanki, Natalie Krivova

4.1.2.4.1 General characteristics

Faculae is the name given to brightenings seen in photospheric radiation (e.g., in visible continuum radiation) mainly near the limb of the Sun (Fig. 1), often in the general vicinity of sunspots. The corresponding brightenings in chromospheric radiation (e.g., in the cores of strong lines, such as Ca II H and K) are termed plage. In contrast to faculae, plage are almost equally well visible at all positions on the solar disc. In general, plage and faculae are found in active regions, although in weaker form similar brightenings are also observed in the quiet Sun, forming a network at the borders of supergranule cells.

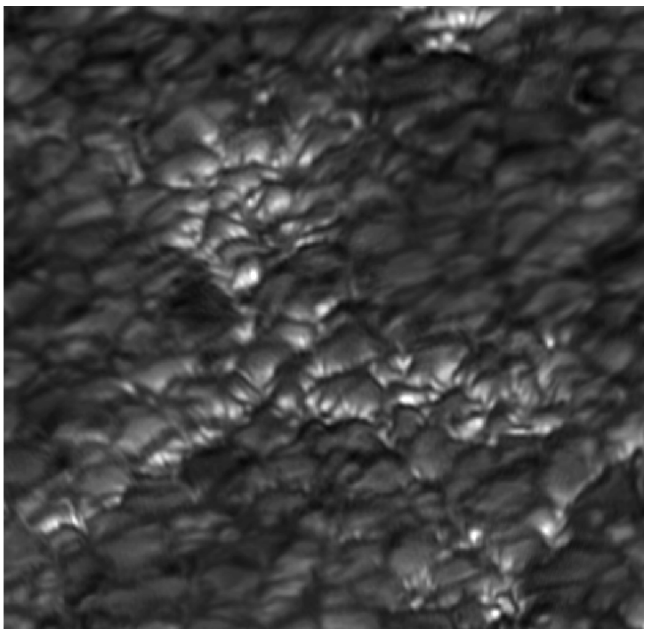

Fig. 1. Faculae near the solar limb. Detail of an image taken at the Swedish Solar Telescope by V. Zakharov.

Faculae, plage and network brightenings are manifestations of concentrated magnetic fields, conglomerates of magnetic elements, each less than a few hundred km in diameter. The individual flux concentrations underlying faculae and plage are significantly smaller than those that form pores and sunspots [a, b].

At high resolution faculae are found to be composed of facular granules (granules that are particularly bright on the side pointing towards solar disc centre), which are most common near the limb, while closer to solar disc centre continuum bright points are more common (roughly at $\mu > 0.7$, where $\mu = \cos\theta$ and θ is the angle between the line of sight and the surface normal).

4.1.2.4.2 Location and size

The strongest faculae and plage are restricted to the acitivity belts, i.e. to within 40° of the equator, although network brightenings are found over the whole solar disc. Near the poles a

larger concentration of intense faculae can be found (so-called polar faculae) during the minimum phase of the sunspot cycle.

In the quiet Sun, the network elements are restricted to the boundaries of the supergranule cells, i.e. the cell size of the network is typically 20-40 Mm. In active regions, the magnetic features tend to form smaller, mesogranulation-sized cells. On a more localized scale, the magnetic elements that form both faculae and the network are located in the downflow lanes between granules [87Tit, 89Sol]. Only magnetic flux concentrations below a certain diameter of 300-400 km are bright at most wavelengths. Larger features, small pores, can be dark in the continuum, but appear bright when radiation from line cores or near the limb is considered.

In addition to the magnetic elements forming faculae and the network there is also another type of magnetic feature ubiquitous in the quiet Sun, the internetwork fields. These display at most a rather subtle brightness signature.

4.1.2.4.3 Intensity and temperature structure

The brightness of faculae, bright points, plage etc. depends strongly on wavelength, on $\mu = \cos\theta$, on the magnetic flux (averaged magnetic field strength $\langle B \rangle$) of the studied magnetic feature and on spatial resolution. Consequently, it is not surprising that different studies have provided such diverse results, e.g., [a, 93Law, 97Top, 02Ort, 04Fou, 07Erm]. The dependence on wavelength suggests that the temperature gradient in faculae is different from that in the quiet Sun (see below); the dependence on spatial resolution is explained by the fact that the contrast of faculae is due to the high contrast of smaller features (magnetic elements, etc.) composing them. Finally, the non-linear dependence on $\langle B \rangle$ implies that as $\langle B \rangle$ increases the average properties of features change.

The dependence of the continuum contrast of network and faculae at 6768 Å at a constant spatial resolution of $4''$ on both $\mu = \cos\theta$ (i.e. the CLV of the contrast) and $\langle B \rangle$ can be expressed by the equation [02Ort]:

$$\begin{aligned} C_{\rm fac}(\mu, \langle B \rangle/\mu) = {} & 10^{-4}\left[0.48 + 9.12\mu - 8.50\mu^2\right](\langle B \rangle/\mu) \; + \\ & 10^{-6}\left[0.06 - 2.00\mu + 1.23\mu^2\right](\langle B \rangle/\mu)^2 + \\ & 10^{-10}\left[0.63 + 3.90\mu + 2.82\mu^2\right](\langle B \rangle/\mu)^3 . \end{aligned} \tag{1}$$

Features with strong $\langle B \rangle$ are dark in the continuum-forming layer, but are bright when we consider spectral line cores, in particular lines whose cores are formed in the chromosphere (and the line is sufficiently temperature sensitive). Integrated over a wide range of wavelengths and over the faculae present on the disc at the time of observation, the CLV of facular contrast relative to the quiet Sun, C, observed with a diffraction limited telescope with a diameter of 30 cm can be expressed as [04Fou]:

$$C(\mu) - 1 = (0.0157 \pm 0.0009)/\mu) + (-0.0075 \pm 0.0003)\,, \tag{2}$$

where

$$C(\mu) = I_{\rm fac}(\mu)/I_{\rm quiet\ Sun}(\mu). \tag{3}$$

Contrast depends on wavelength, λ, roughly as $1/\lambda$ [77Cha], although a number of spectral features cause significant deviation from this dependence at given wavelengths e.g. [99Unr] (Fig. 2). The contrast of faculae is larger in wavelength bands at which molecular lines enhance the contrast, e.g., the G-band or the CN band head. Contrast values measured at high resolution at these wavelengths (Swedish Solar Telescope) are given in Table 1 [05Zak]. There is evidence that at a wavelength of 1.6 μm in the infrared faculae actually appear dark [92Mor]. Brightness depends

Table 1. Contrasts of magnetic bright points at different wavelengths

Wavelength band	Continuum	G-band	CN-band head
Contrast	0.14	0.34	0.48

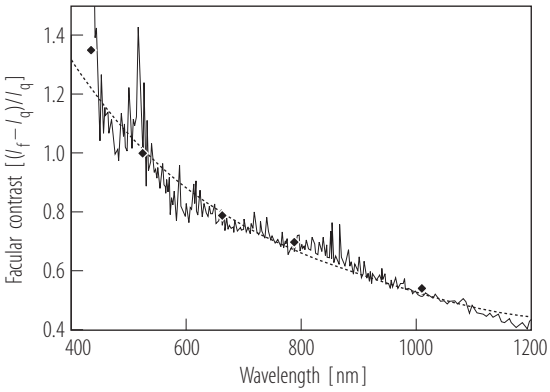

Fig. 2. The spectral variation of the facular contrast calculated by [99Unr] (solid line) and measured by [77Cha] (diamonds). The measurements were done between 16 and 53″of the limb ($\mu = 0.18$ to 0.33). The dotted line shows the inverse wavelength fit suggested by [77Cha].

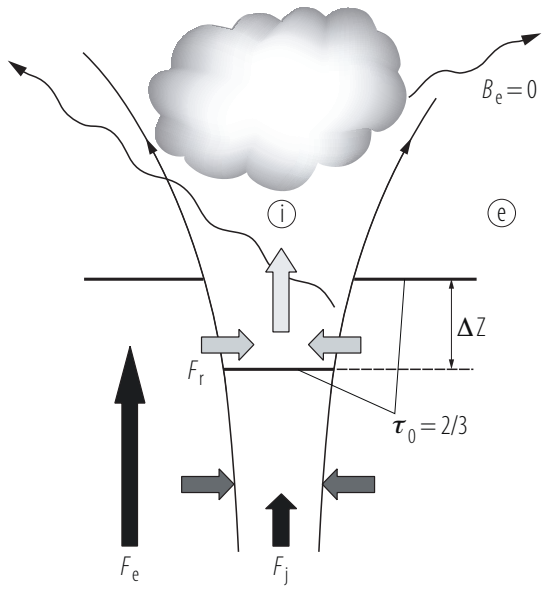

Fig. 3. Sketch of a magnetic flux tube and the processes leading to excess radiation emerging from it in the photosphere and the chromosphere. See text for details. Adapted from [78Zwa].

strongly on the size of a magnetic feature. In the visible, magnetic elements with diameters less than 300-400 km are brighter than average quiet Sun, while larger features are darker (micropores, pores).

Faculae and plage are bright because they are hotter than their surroundings at equal optical depth. The temperature structure has been deduced empirically (and also results from MHD simulations). In Table 2 empirical model atmospheres for magnetic elements in faculae (active regions) and the network (quiet Sun) are listed. These models have been deduced from Fourier Transform Spectrometer data [84Ste] by [86Sol, 92Sol] under the assumption of LTE (Local Thermodynamic Equilibrium). Models including a chromospheric temperature rise have been published by [95Bri], cf. [93Bru].

The dependence of the brightness or contrast on magnetic flux in the resolution element can be at least qualitatively understood by considering the sketch shown in Fig. 3 [07Sol], adapted from a figure in [78Zwa]. It shows a schematic magnetic flux tube (the boundaries or side walls of the

Table 2. Network magnetic element model atmosphere [92Sol]. τ is the continuum optical depth at 500 nm, Z is height, with $Z = 0$ corresponding to the average $\tau = 1$ in the quiet Sun, T is temperature, $P_{\rm gas}$ the gas pressure and B the field strength.

$\log(\tau)$	Z [cm]	T [K]	$P_{\rm gas}$ [CGS]	B [G]
–4.06	4.18E+07	4724.4	1.035E+03	251.1
–3.93	4.00E+07	4733.2	1.217E+03	275.2
–3.80	3.80E+07	4744.5	1.445E+03	301.7
–3.67	3.63E+07	4783.3	1.691E+03	329.8
–3.54	3.45E+07	4798.0	1.981E+03	359.8
–3.41	3.27E+07	4807.6	2.328E+03	393.2
–3.28	3.09E+07	4809.8	2.736E+03	428.0
–3.15	2.91E+07	4814.7	3.214E+03	465.8
–3.02	2.72E+07	4829.7	3.779E+03	507.4
–2.89	2.54E+07	4846.7	4.446E+03	552.8
–2.76	2.35E+07	4861.0	5.233E+03	602.3
–2.63	2.17E+07	4874.2	6.144E+03	653.5
–2.50	1.98E+07	4889.4	7.239E+03	710.4
–2.37	1.80E+07	4905.9	8.484E+03	767.3
–2.24	1.62E+07	4946.4	9.949E+03	829.7
–2.11	1.44E+07	4986.5	1.164E+04	896.3
–1.98	1.25E+07	5055.9	1.369E+04	970.4
–1.85	1.05E+07	5253.8	1.604E+04	1048.9
–1.72	8.73E+06	5427.1	1.854E+04	1126.1
–1.59	7.08E+06	5572.7	2.108E+04	1200.9
–1.46	5.43E+06	5666.9	2.390E+04	1278.4
–1.33	3.78E+06	5761.2	2.704E+04	1359.2
–1.20	2.13E+06	5861.6	3.053E+04	1441.2
–1.07	5.93E+05	5964.4	3.411E+04	1518.6
–0.94	–1.02E+06	6081.4	3.824E+04	1599.4
–0.81	–2.53E+06	6188.0	4.249E+04	1672.8
–0.69	–4.02E+06	6297.2	4.706E+04	1740.0
–0.56	–5.52E+06	6415.6	5.203E+04	1801.9
–0.43	–7.13E+06	6541.5	5.784E+04	1863.0
–0.30	–8.63E+06	6658.8	6.375E+04	1915.2
–0.17	–1.01E+07	6785.3	7.011E+04	1962.8
–0.04	–1.16E+07	6922.5	7.714E+04	2007.1
0.09	–1.30E+07	7095.1	8.395E+04	2043.6
0.22	–1.45E+07	7279.9	9.147E+04	2078.4
0.35	–1.59E+07	7468.9	9.935E+04	2109.4
0.48	–1.72E+07	7662.3	1.071E+05	2135.7
0.61	–1.86E+07	7864.9	1.157E+05	2160.6
0.74	–1.99E+07	8085.0	1.238E+05	2181.1
0.87	–2.12E+07	8361.1	1.323E+05	2199.2
1.00	–2.24E+07	8700.9	1.404E+05	2215.0

flux tube are represented by the curved, nearly vertical lines) passing through the solar surface (the thick horizontal lines). Note that the solar surface lies at a lower level in the flux tube due to its evacuation, which is a consequence of horizontal pressure balance (height difference ΔZ, which is typically 100-200 km). In the subphotosphere the magnetic field leads to a reduction in the efficiency of convection (heat blocking), indicated in Fig. 3 by the black vertical arrows (internal

vertical energy flux $F_i \ll F_e$; note that subscripts i refer to the interior of the flux tube, subscripts e to the exterior). This is compensated by the lateral inflow of radiation into the flux tube (F_r) through the walls at a level lying between the internal $\tau = 1$ surface and the external $\tau = 1$ surface, indicated by the upper pair of horizontal (grey shaded) arrows. For a strong field that almost completely blocks the internal convective transport, to first order the amount of heating depends on the ratio of the wall area to the area of the flux tube's cross section.

If the flux tube is small, then the inflowing radiation can more than compensate the blocked vertical energy flux, leading to a positive contrast of the magnetic features. This simple model also, at least qualitatively, explains the centre-to-limb behaviour of the contrast, in particular the brightening seen away from disc centre, as the hot walls become visible (indicated in Fig. 3 by the long wavy arrow leaving the right wall towards the upper left).

In the chromosphere plage display an increase of the contrast relative to the quiet Sun vs. $\langle B \rangle$, the spatially averaged field strength in the resolution element. Quantitatively, the line core excess flux density of the H &K lines of Ca II, $\Delta F_{\mathrm{Ca\,II}}$ (erg cm^{-2} s^{-1}), can be written as [89Sch]:

$$\log \Delta F_{\mathrm{Ca\,II}} = 0.6 \log\langle B \rangle + 4.8. \quad (4)$$

The contrast in the core of Ca II H and K is almost independent of μ.

In addition to radiation, mechanical energy is laterally introduced into the magnetic feature by the turbulent medium in which it is embedded [96Ste]. Convection excites different MHD wave modes that travel up along the field, e.g., [95Hua]. These can be longitudinal, tube waves, e.g., [78Rob, 00Mus], transverse modes [02Mus] or torsional Alfvén waves [03Nob]. See e.g., [96Nar, 97Rob, 05Car] for overviews. The energy input by the granular buffeting is indicated in Fig. 3 by the lower pair of horizontal (hatched) arrows.

These waves carry a given energy flux into the chromosphere, indicated by the upper vertical arrow. The energy in the magneto-acoustic tube mode can be dissipated in the chromospheric layers through the formation of shocks [85Her, 98Faw]. The dissipation region is indicated by the shaded cloud (of hot gas) in Fig. 3.

The increase in the contrast with magnetic flux is explained by the increasing density of magnetic flux tubes as the magnetic flux increases [91Sol, 98Faw] and the gradual saturation of the chromospheric contrast by a decreased excitation rate of waves as a large density of flux tubes starts affecting the granules around them [89Tit].

4.1.2.4.4 B-field structure

Generally, faculae are composed mainly of magnetic elements and larger concentrations of magnetic flux that are described by magnetic flux tubes (see Fig. 3). Since the magnetic elements forming faculae are usually not spatially resolved by present-day observations, there is a dichotomy between the apparent field strength as obtained from magnetograms and the intrinsic field strength in the elements. Apparent field strength depends on the spatial resolution of the observations. Intrinsic magnetic field strengths lie between 1000 G and 1500 G for active region faculae observed in the visible at a height corresponding to the mid-photosphere. The intrinsic field strengths are always higher than (or equal to) the apparent (i.e. spatially averaged) field strength. The difference between intrinsic and averaged field strength implies that the magnetic features fill only a fraction of the solar surface within a spatial resolution element. This coverage fraction is termed the magnetic filling factor.

The field strength in magnetic elements is strongly height dependent and can be deduced from measurements carried out in different spectral lines. In the deep photosphere, the field strength is around 1500-1700 G [92Rab, 92Rue], dropping to roughly 1300-1400 G in the lower-middle photosphere, sampled by the Fe I 6301 Å and 6302 Å line pair [97Mar], to 1000-1200 G in the upper middle photosphere [85Ste], and to 200-500 G near the temperature minimum [89Zir, 95Bru]. The results agree well with the thin-tube approximation, according to which the field strength follows

Table 3. Plage magnetic element model atmosphere [92Sol].

$\log(\tau)$	Z [cm]	T [K]	$P_{\rm gas}$ [CGS]	B [G]
–4.06	3.74E+07	4619.1	1.043E+03	331.3
–3.93	3.57E+07	4635.0	1.225E+03	359.6
–3.80	3.40E+07	4655.3	1.439E+03	391.1
–3.67	3.22E+07	4675.6	1.691E+03	425.4
–3.54	3.05E+07	4695.8	1.986E+03	459.9
–3.41	2.87E+07	4716.0	2.333E+03	499.9
–3.28	2.70E+07	4735.9	2.740E+03	540.4
–3.15	2.52E+07	4754.2	3.219E+03	587.2
–3.02	2.34E+07	4774.9	3.782E+03	637.9
–2.89	2.16E+07	4796.0	4.443E+03	690.0
–2.76	1.98E+07	4815.5	5.221E+03	748.5
–2.63	1.80E+07	4832.1	6.136E+03	807.4
–2.50	1.62E+07	4850.8	7.211E+03	870.6
–2.37	1.44E+07	4867.5	8.476E+03	938.4
–2.24	1.26E+07	4885.2	9.963E+03	1010.6
–2.11	1.07E+07	4907.3	1.171E+04	1092.3
–1.98	8.86E+06	4928.1	1.377E+04	1169.4
–1.85	6.96E+06	4947.7	1.620E+04	1256.9
–1.72	5.16E+06	5020.1	1.905E+04	1340.8
–1.59	3.26E+06	5172.4	2.238E+04	1435.4
–1.46	1.36E+06	5337.2	2.611E+04	1530.5
–1.33	–4.39E+05	5517.3	3.012E+04	1622.2
–1.20	–2.04E+06	5698.2	3.424E+04	1696.5
–1.07	–3.64E+06	5802.3	3.859E+04	1756.4
–0.94	–5.24E+06	5854.1	4.355E+04	1821.2
–0.81	–6.94E+06	5896.5	4.938E+04	1884.5
–0.69	–8.64E+06	5931.2	5.571E+04	1944.2
–0.56	–1.05E+07	5977.8	6.376E+04	2001.6
–0.43	–1.24E+07	6014.0	7.324E+04	2062.4
–0.30	–1.44E+07	6050.4	8.446E+04	2117.6
–0.17	–1.64E+07	6106.6	9.756E+04	2172.7
–0.04	–1.84E+07	6170.6	1.126E+05	2216.8
0.09	–2.04E+07	6275.1	1.293E+05	2260.0
0.22	–2.23E+07	6403.1	1.472E+05	2293.2
0.35	–2.41E+07	6561.3	1.659E+05	2335.0
0.48	–2.57E+07	6755.1	1.846E+05	2381.4
0.61	–2.72E+07	6993.9	2.028E+05	2401.7
0.74	–2.85E+07	7280.8	2.197E+05	2418.8
0.87	–2.97E+07	7617.6	2.348E+05	2437.0
1.00	–3.06E+07	8081.0	2.474E+05	2447.6

horizontal pressure balance. Typical dependences of field strength on height for a thin flux tube are given in Tables 2 and 3.

Whereas the temperature is a strong function of the magnetic filling factor, the intrinsic magnetic field strength depends less: B changes by 10-20% as the filling factor (or magnetic flux per spatial resolution element) changes by a factor of 5-10. For very small flux per pixel (2×10^{16} Mx/(arc sec)^2), as typical of the internetwork region of the quiet Sun, the field strength becomes significantly smaller. Fields of 600 G or less are measured there [03Kho, 07Oro].

4.1.2.4.5 Velocity structure

Velocities within the magnetic features of faculae are given by the zero-crossing wavelengths of Stokes V profiles. These are within 200-300 $\mathrm{m\,s^{-1}}$ of zero, so that at the heights of formation of the cores of these lines no strong downflows are present [86Sol, 97Mar]. In the deep photospheric layers of magnetic elements, strong downflows of multiple km/s have been deduced [04Bel]. The data can be reproduced without them as well [98Fru].

The magnetic elements are embedded in the downflow lanes bounding the granules. This leads to the production of strongly asymmetric Stokes V profiles [88Gro, 89Sol] in the sense that, at disc centre, the blue lobes are larger than the red lobes both in amplitude and in area [84Ste, 84Sol]. The relative difference depends on the region and the spectral line, but is typically 5-10%, although much larger asymmetries are also known. Towards the limb the asymmetry of the Stokes V wing areas reverses sign [87Ste, 97Mar].

4.1.2.4.6 References for 4.1.2.4

General references

a Solanki, S.K.: Space Sci. Rev. **63** (1993) 1.

b Stenflo, J.O.: Solar Magnetic Fields: Polarized Radiation Diagnostics, Dordrecht: Kluwer (1994).

Special references

77Cha Chapman, G.A., McGuire, T.E.: Astrophys. J. **217** (1977) 657.

78Rob Roberts, B., Webb, A.R.: Sol. Phys. **56** (1978) 5.

78Zwa Zwaan, C.: Sol. Phys. **60** (1978) 213.

84Sol Solanki, S.K., Stenflo, J.O.: Astron. Astrophys. **140** (1984) 185.

84Ste Stenflo, J.O., Solanki, S.K., Harvey, J.W., Brault, J.W.: Astron. Astrophys. **131** (1984) 333.

85Her Herbold, G., Ulmschneider, P., Spruit, H.C., Rosner, R.: Astron. Astrophys. **145** (1985) 157.

85Ste Stenflo, J.O., Harvey, J.W.: Sol. Phys. **95** (1985) 99.

86Sol Solanki, S.K.: Astron. Astrophys. **168** (1986) 311.

87Ste Stenflo, J.O., Solanki, S.K., Harvey, J.W.: Astron. Astrophys. **171** (1987) 305.

87Tit Title, A.M., Tarbell, T.D., Topka, K.P.: Astrophys. J. **317** (1987) 892.

88Gro Grossmann-Doerth, U., Schüssler, M., Solanki, S. K.: Astron. Astrophys. **206** (1988) L37.

89Sch Schrijver, C.J., Cote, J., Zwaan, C., Saar, S.H.: Astrophys. J. **337** (1989) 964.

89Sol Solanki, S.K.: Astron. Astrophys. **224** (1989) 225.

89Tit Title, A.M., Tarbell, T.D., Topka, K.P., Ferguson, S.H., Shine, R.A., & SOUP Team: Astrophys. J. **336** (1989) 475.

89Zir Zirin, H., Popp, B.: Astrophys. J. **340** (1989) 571.

91Sol Solanki, S.K., Steiner, O., Uitenbroeck, H.: Astron. Astrophys. **250** (1991) 220.

92Mor Moran, T., Foukal, P., Rabin, D.: Sol. Phys. **142** (1992) 35.

92Rue Rüedi, I., Solanki, S.K., Livingston, W., Stenflo, J.O.: Astron. Astrophys. **263** (1992) 323.

92Rab Rabin, D.: Astrophys. J. **391** (1992) 832.

92Sol Solanki, S.K., Brigljevic, V.: Astron. Astrophys. **262** (1992) L29.

93Bru Bruls, J.H.M.J., Solanki, S.K.: Astron. Astrophys. **273** (1993) 293.

93Law Lawrence, J.K., Topka, K.P., Jones, H.P.: J. Geophys. Res. **98** (1993) 18 911.

95Bri Briand, C., Solanki, S.K.: Astron. Astrophys. **299** (1995) 596.
95Bru Bruls, J.H.M.J., Solanki, S.K.: Astron. Astrophys. **293** (1995) 240.
95Hua Huang, P., Musielak, Z.E., Ulmschneider, P.: Astron. Astrophys. **297** (1995) 579.
96Nar Narain, U., Ulmschneider, P.: Space Sci. Rev. **75** (1996) 453.
96Ste Steiner, O., Grossmann-Doerth, U., Schüssler, M., Knolker, M.: Sol. Phys. **164** (1996) 223.
97Mar Martínez Pillet, V., Lites, B.W., Skumanich, A.: Astrophys. J. **474** (1997) 810.
97Rob Roberts, B., Ulmschneider, P.: In: European Meeting on Solar Physics, Eds.: Simnett, G.M. and Alissandrakis, C.E. and Vlahos, L., Lecture Notes Phys. **489** (1997) 75.
97Top Topka, K.P., Tarbell, T.D., Title, A M.: Astrophys. J. **484** (1997) 479.
98Faw Fawzy, D.E., Ulmschneider, P., Cuntz, M.: Astron. Astrophys. **336** (1998) 1029.
98Fru Frutiger, C., Solanki, S.K.: Astron. Astrophys. **336** (1998) L65.
99Unr Unruh, Y.C., Solanki, S.K., Fligge, M.: Astron. Astrophys. **345** (1999) 635.
00Mus Musielak, Z.E., Rosner, R., Ulmschneider, P.: Astrophys. J. **541** (2000) 410.
02Mus Musielak, Z.E., Ulmschneider, P.: Astron. Astrophys. **386** (2002) 606.
02Ort Ortiz, A., Solanki, S.K., Domingo, V., Fligge, M., Sanahuja, B.: Astron. Astrophys. **388** (2002) 1036.
03Kho Khomenko, E.V., Collados, M., Solanki, S.K., Lagg, A., Trujillo Bueno, J.: Astron. Astrophys. **408** (2003) 1115.
03Nob Noble, M.W., Musielak, Z.E., Ulmschneider, P.: Astron. Astrophys. **409** (2003) 1085.
03Wal Walton, S.R., Preminger, D.G., Chapman, G.A.: Sol. Phys. **213** (2003) 301.
04Bel Bellot Rubio, L.R., Ruiz Cobo, B., Collados, M.: Astrophys. J. **611** (2004) L57.
04Fou Foukal, P., Bernasconi, P., Eaton, H., Rust, D.: Astrophys. J. **611** (2004) L57.
05Car Carlsson, M., Hansteen, V.: in: Chromospheric and Coronal Magnetic Fields, Eds.: Innes, D.E. and Lagg, A. and Solanki, S.K., ESA SP-596 (2005) 39.1.
05Zak Zakharov, V., Gandorfer, A., Solanki, S.K., Löfdahl, M.: Astron. Astrophys. **437** (2005) L43.
07Erm Ermolli, I., Criscuoli, S., Centrone, M., Giorgi, F., Penza, V.: Astron. Astrophys. **465** (2007) 305.
07Oro Orozco Suárez, D., Bellot Rubio, L.R., del Toro Iniesta, J.C. et al.: Astrophys. J. Lett. **670** (2007) L61.
07Sol Solanki, S.K.: In: The Physics of Chromospheric Plasmas, Eds.: P. Heinzel, I. Dorotovič, and R. J. Rutten, San Francisco: Astronomical Society of the Pacific, ASP Conference Series **368** (2007) 481.